PAPER

InSe monolayer: synthesis, structure and ultra-high second-harmonic generation

To cite this article: Jiadong Zhou *et al* 2018 *2D Mater.* **5** 025019

2D Materials

PAPER

RECEIVED
25 November 2017

REVISED
13 February 2018

ACCEPTED FOR PUBLICATION
2 March 2018

PUBLISHED
20 March 2018

InSe monolayer: synthesis, structure and ultra-high second-harmonic generation

Jiadong Zhou[1], Jia Shi[2], Qingsheng Zeng[1], Yu Chen[3], Lin Niu[1], Fucai Liu[1], Ting Yu[3], Kazu Suenaga[4], Xinfeng Liu[2], Junhao Lin[4] and Zheng Liu[1,5,6,7]

[1] Centre for Programmable Materials, School of Materials Science and Engineering, Nanyang Technological University, Singapore 639798, Singapore
[2] CAS Key Laboratory of Standardization and Measurement for Nanotechnology, CAS Center for Excellence in Nanoscience, National Center for Nanoscience and Technology, Beijing 100190, People's Republic of China
[3] Centre for Disruptive Photonic Technologies, School of Physical and Mathematical Sciences, Nanyang Technological University, Singapore 637371, Singapore
[4] National Institute of Advanced Industrial Science and Technology (AIST), Tsukuba 305-8565, Japan
[5] Centre for Micro-/Nano-electronics (NOVITAS), School of Electrical and Electronic Engineering, Nanyang Technological University, 50 Nanyang Avenue, Singapore 639798, Singapore
[6] CINTRA CNRS/NTU/THALES, UMI 3288, Research Techno Plaza, 50 Nanyang Drive, Border X Block, Level 6, Singapore 637553, Singapore
[7] Environmental Chemistry and Materials Centre, Nanyang Environment and Water Research Institute, 1 Cleantech Loop, Singapore 637141, Singapore

E-mail: z.liu@ntu.edu.sg **and** lin.junhao.stem@gmail.com

Keywords: InSe, 2D materials, physical vapor deposition, second-harmonic generation

Supplementary material for this article is available online

Abstract

III–IV layered materials such as indium selenide have excellent photoelectronic properties. However, synthesis of materials in such group, especially with a controlled thickness down to monolayer, still remains challenging. Herein, we demonstrate the successful synthesis of monolayer InSe by physical vapor deposition (PVD) method. The high quality of the sample was confirmed by complementary characterization techniques such as Raman spectroscopy, atomic force microscopy (AFM) and high resolution annular dark field scanning transmission electron microscopy (ADF-STEM). We found the co-existence of different stacking sequence (β- and γ-InSe) in the same flake with a sharp grain boundary in few-layered InSe. Edge reconstruction is also observed in monolayer InSe, which has a distinct atomic structure from the bulk lattice. Moreover, we discovered that the second-harmonic generation (SHG) signal from monolayer InSe shows large optical second-order susceptibility that is 1–2 orders of magnitude higher than MoS_2, and even 3 times of the largest value reported in monolayer GaSe. These results make atom-thin InSe a promising candidate for optoelectronic and photosensitive device applications.

Introduction

2D materials have attracted intense attention due to their excellent physical properties, such as high mobility, on/off current ratio and the tunable band gap [1, 2], which make them potential candidates for the next generation applications in flexible transparent electrodes, photonics sensors, conductive composites, gas separation membranes and nonlinear optics [3–8]. The zero band gap of graphene limits its application in field effect transistors (FET) [9]. As a result, many works have been done in the fields of semiconducting TMDs such as MoS_2, WS_2, $MoSe_2$ and WSe_2, exploring large scale synthetic methods and unique properties of these TMDs [10–14]. As a comparison, IIIA-VIA layered materials such as GaS, GaSe, In_2Se_3 and InSe also show potential applications for next generation electronics and optoelectronics due to their suitable bandgaps [15–18]. In particular, ultra-high mobility of 1000 $cm^2 V^{-1} s^{-1}$ in multilayer InSe transistors was reported by Hu's group [19], quantum hall effect and anomalous response were realized in atomically thin-atom InSe [20], and high performance photodetectors based on few-layered InSe or InSe/graphene heterostructure have been demonstrated [17, 21–23]. Besides the optoelectronic and photosensitive device applications, InSe has also been considered as a promising candidate to accommodate nonlinear optical effect. Especially,

monolayer InSe offers the possibility to study the second-order optical nonlinearity due to the lack of an inversion center.

Second-harmonic generation (SHG) effect is a nonlinear optical effect. It refers to a process that two photons with the same frequency are effectively combined inside the material, emitting one new photon with twice of the energy and frequency of the initial photon. Such effect is often observed in crystals with nonlinear dielectric response matrix. Recently, nonlinear optical effects in monolayer materials have attracted intensive attentions. The SHG effect in 2D monolayer such as graphene, WSe_2, MoS_2, GaSe and few layer InSe have been studied [24–28]. However, the SHG effect in monolayer InSe has not been investigated yet. Exploring the strong nonlinear effect in monolayer InSe is of great importance in expanding its potential applications. As the first step, access to large-scale InSe with good thickness control is necessary. So far, high quality monolayer IIIA-VIA materials are produced mainly by chemical or mechanical exfoliation from their bulk counterparts, which, however, are in low yield and with poor thickness control. Although the synthesis of monolayer GaSe and In_2Se_3 have been reported [29–31], the synthesis of monolayer InSe still remains challenging. The difficulties in synthesizing monolayer InSe originates from the fact that rich phases of In_xSe_y are easily produced at high temperatures, such as InSe, $InSe_2$, In_2Se_3, In_3Se_4 and so on [32, 33], making the process hard to control. Moreover, the decomposition of InSe at high temperatures is another barrier to produce high quality InSe monolayer [34]. A recent literature reported synthesis of InSe film by pulsed laser deposition (PLD) [35], but there is little effort in exploring other possible routes to obtain InSe layers in large scale.

Here, we report the successful synthesis of large-size monolayer InSe by physical vapor deposition (PVD) method. The size of InSe is up to 40 μm and the thickness can be controlled by growth time. Temperature dependent Raman spectra demonstrates the high quality of the as-synthesized InSe films. The atomic structures of InSe, including monolayer, few-layer and edges, were identified by scanning transmission electron microscope (STEM). The monolayer InSe exhibits strong second-harmonic generation signal and the few-layer InSe FET shows good photoelectronic properties.

Methods

Synthesis of InSe atomic layers

In our experiment, the silica boat containing InSe (99.99%, Alfar) powder (20 mg) was put in the center of the tube. A piece of Si wafer with 285 nm SiO_2 top layer was placed in the downstream about 10–15 cm far away, served as the substrate for the sample growth. Argon flow of 60 standard cubic centimeters per second (sccm) provide an inert atmosphere, and also carried the vaporized InSe gas to deposit on the surface of SiO_2/Si. The InSe powder was heated to 830 °C in 30 min and kept at 830 °C for 5 min to 20 min for the growth of InSe atomic layers. Then the system was cooled down to room temperature.

Raman measurement

Raman measurement with the excitation laser of 532 nm was performed using a WITEC alpha 200R Confocal Raman system. Before Raman characterization, the system was calibrated with the Raman peak of Si at 520 cm^{-1}. The Raman mapping was performed on the same system with the same laser line. The laser powers are less than 1 mW.

SHG measurement

The output from a mode-locked Ti:sapphire laser (output wavelength: 800 nm and repetition rate: 76 MHz) was filtered, attenuated, and focused on a sample by microscope objective lens (100×, NA = 0.95, with spot size ~1.6 μm at fundamental wavelength). The SHG signal was then back collected by the same lens, separated using a dichroic mirror, and filtered by a 650 nm short pass filter before entering a spectrometer (PI Acton 2500i with a liquid nitrogen cooled charge coupled device—CCD camera). To measure the polarization dependence of the SHG signal, the fundamental beam was first prepared in a linear polarization state using a polarizer. By placing a linear polarizer in front of the spectrometer, we measure x and y components as a function of θ, the angle between crystal axis and the polarization angle of incident light, by rotating the sample about the z axis.

STEM sample preparation and characterization

The STEM samples were prepared with a poly (methyl methacrylate) (PMMA) assisted method. A layer of PMMA of about 1 μm thick was spin-coated on the wafer with InSe samples deposited, and then baked at 170 °C for 5 min. Then the wafer was immersed in KOH solution (1 M) to etch the SiO_2 layer over night. After lifting off, the PMMA/InSe film was transferred to DI water for several cycles to wash away the residual contaminations, and then it was fished by a TEM grid (Quantifoil Mo grid). The transferred specimen was dried naturally in ambient environment, and then dropped into the acetone overnight to wash away the PMMA coating layers. The monolayers were transferred on to transmission electron microscope (TEM) microgrids. STEM imaging and EELS chemical analysis was performed by JEOL 2100F equipped with Delta correctors and GIF quantum spectrometer, operated at 60 kV. The inner and outer collection angles for the STEM image (β1 and β2) were 62 and 129–140 mrad, respectively, with a convergence semi-angle of 35 mrad.

Device fabrication and characterization

The as-grown InSe few layer was patterned to a rectangle with UV-lithography and oxygen plasma,

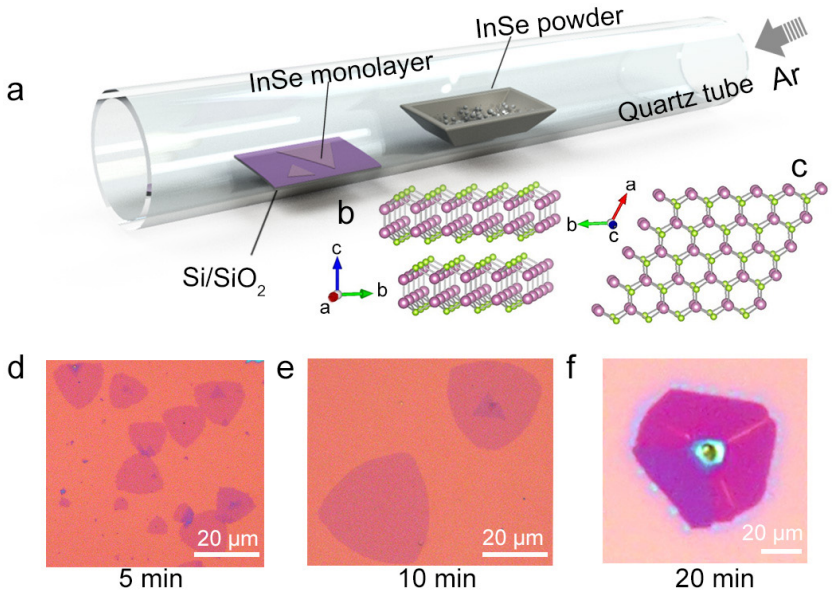

Figure 1. PVD setup and optical images of atomically layered InSe. (a) InSe layers synthesized via PVD method using the InSe powder as precursor. SiO_2/Si wafer was used as a substrate. (b) and (c) Crystal structure of InSe. The purple balls refer to indium atoms and selenium atoms are in green. InSe shows a hexagonal structure with single layer symmetry of D 3 h. The lattice constant along *a* or *b* axis is 0.40 nm and the distance between two neighboring layers is around 0.8 nm. (d)–(f) Optical images of InSe with different grow time of 5 min, 10 min, and 20 min, respectively. Monolayer InSe can be obtained for a short-time growth less than 10 min (d) and (e) and few-layer InSe can be produced for a longer reaction time (f).

then 5/50 nm Cr/Au layers were deposited on the rectangle with E-beam vapor deposition as electrodes with UV-lithography. The optical image of the fabricated device is shown in figure 6(a). The devices were measured with a probe station in a vacuum chamber.

Results and discussion

Figure 1(a) shows the reaction system that was used to synthesize InSe layers. The InSe powder was used as the source and Ar as the carrier gas. The details of the synthetic method can be found in the Methods section. Figures 1(b) and (c) illustrate the crystal structure of InSe with Se–In–In–Se bonding in one layer. Figures 1(d)–(f) display the optical images of InSe with different sizes and layers by controlling the growth time at the growth temperature of 830 °C. In our experiment, the distance between the source and substrate is about 12 cm. The size of monolayer InSe can reach up to 40 μm when the growth time is 10 min. Note that the size of monolayer InSe is small when the growth time is less than 5 min. As the growth time increases, few-layer InSe starts to appear, which are shown in figure 1(f). More optical images of InSe flakes with different thickness under different growth time are shown in figure S1 (stacks.iop.org/TDM/5/025019/mmedia). The corresponding scanning electron microscopy (SEM) images of monolayer InSe are shown in figure S2, showing a homogenous morphology.

Figure 2(a) shows the optical image of InSe film with size up to 30 μm, the corresponding AFM image shown in figure 2(b) reveals that the thickness of the film is about 0.8 nm, confirming that the as-synthesized InSe is monolayer [21]. Figures 2(c)–(e) show the optical image and AFM image of InSe with different thickness, ranging from 1 L to 6 L. In order to examine the crystal quality of the as-growth InSe, Raman spectra was used to characterize InSe crystals with 532 nm laser as the excitation source. The Raman spectra of monolayered, 5 layered and 10 layered InSe are shown in figure 2(f). The Raman peaks located at 117 cm^{-1} and 202 cm^{-1} are attributed to the A_1' and A_2'' modes of InSe, respectively, which is consistent with previous report [21]. The temperature dependent Raman spectra of monolayer InSe measured under the same laser power can be found in figure S3, which suggests that the intensity of Raman peaks increases with the temperature decreases. The comparison of Raman peak (A_1' mode) positon under different temperature is shown in figure 2(g). The Raman mapping of A_1' mode is presented in figure S3, showing uniform of the as-grown InSe.

The stability of as-synthesized monolayer and few-layer InSe were further studied in the ambient conditions. Figure 3 shows the optical images of monolayer InSe exposed in air with different time. Optical contrast exhibits that the monolayer InSe decomposes when it was exposed in air for several days. However, the few-layer InSe keeps its shape and contrast as the fresh samples, which are shown in figure S4. Additionally, the Raman spectra of few-layered InSe has no change after exposure in air for 9 d, as shown in figure S4(e). The result demonstrates the stability of the InSe thin film. In contrast, the WTe_2, $MoTe_2$ and

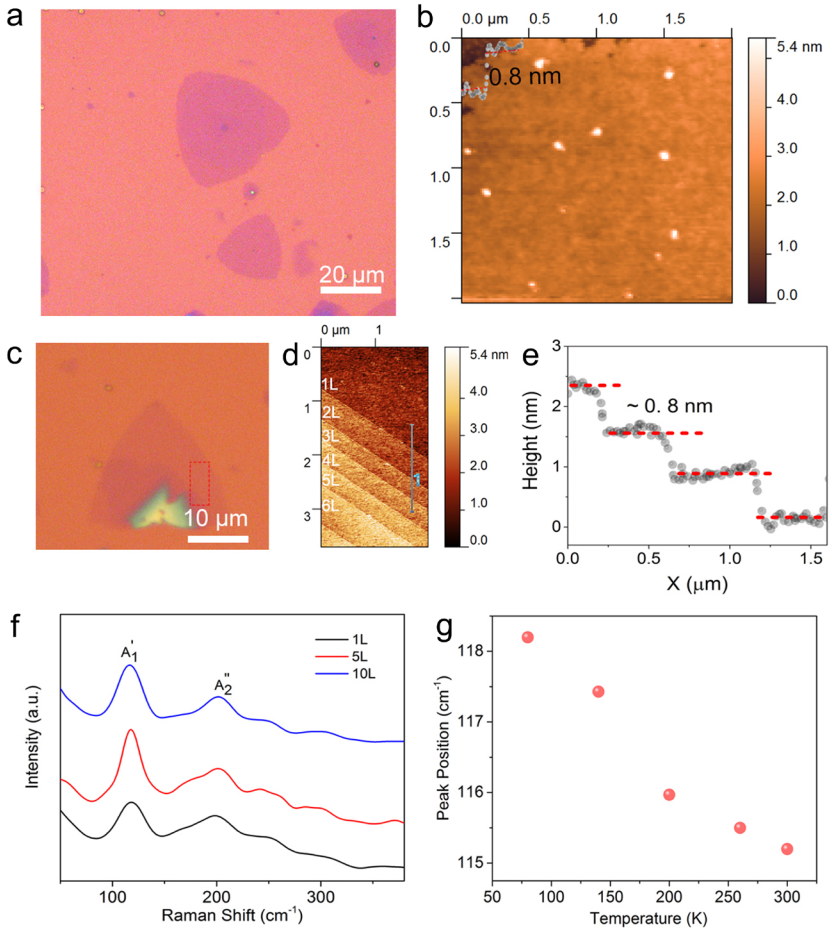

Figure 2. AFM and Raman characterizations of atomically layered InSe. (a) Optical image of large-scale monolayer InSe. (b) Monolayer InSe and the height topography at its edge. The thickness of the flake is around 0.8 nm, confirming that the as-synthesized InSe is monolayer. (c) Optical image of InSe with different layers and the corresponding AFM height topography images shown in (d). The interlayer distance of ~0.8 nm is estimated in (e). (f) Raman spectra of 1 L, 5 L and 10 L InSe. (g) The Raman peak (A_1') position of monolayer InSe dependences of temperature from 80 K to 300 K.

BP decompose quickly when they were exposed in air for few hours [36, 37]. The results indicate that the as-synthesized InSe has higher stability than the BP [36], $MoTe_2$ and WTe_2 [37].

Annual dark-field (ADF) imaging in STEM was used to characterize the quality and crystal structure of InSe film. Figure 4(a) shows an atomic resolution STEM image of the monolayer InSe film. Since the intensity of the STEM image is directly related to the atomic number of the imaged species in the monolayer sample [38], the bright In columns and less bright Se columns are clearly resolved to maintain a hexagonal atomic arrangement in the projected plane along (0 0 1) zone axis. Notably, both In and Se columns have an projected shape of ellipse rather than circle, where the Se columns have longer elliptical axis. This is due to the presence of a small titling angle on the sample, which displaces the In and Se columns. Since InSe maintains a 4 atomic layer structure where two In layer are sandwiched by the other two Se layer, the Se columns have larger displacement than In if a tilting angle presents in the monolayer film, as indicated by the structural models, resulting in a more elliptical shape. The simulated STEM image achieves a good agreement with the experimental image, where the intensity and column shape match quite well as shown in the line intensity profile, further confirming the structural quality of the monolayer InSe film. Figure 4(b) shows the electron energy loss spectrum of the monolayer region, which unambiguously displays the chemical identity of In and Se in the film.

We further explored the atomic structure of few-layer InSe. Bulk InSe has two different phase, β (hexagonal P63/mmc) and Υ (rhombohedral R3m) due to different stacking sequence of individual layers [39]. As the layer of InSe piles up, it can either form β- or γ-InSe depending on the stacking order. Figure 4(c) shows the STEM images of two different stacking orders in few-layer InSe. β-InSe is an analogy of 2H stacking in transition-metal dichalcogenide MX_2 (such as MoS_2) structures where the Se (In) columns in the second layer are well-aligned the In (Se) columns in the first layer. On the other hand, γ-InSe is similar to 3R stacking where the stacking follows the ABCABC patterns, as illustrated by the structural models in figure 4(c). The good agreement of the experimental images with the simulation further confirms the correctness of the models. Therefore, β-InSe and γ-InSe

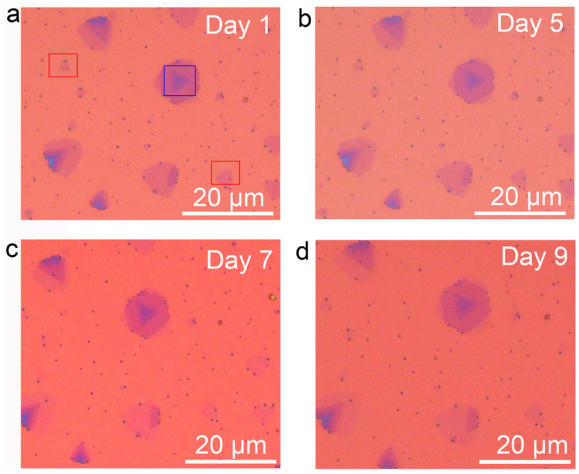

Figure 3. Time-dependent optical images of monolayer InSe. (a) The optical image of freshly PVD synthesized samples, monolayer and few layer InSe are highlighted in red and blue, respectively. (b)–(d), shows the optical image of the samples in (a) after exposed in air 5 d, 7 d and 9 d, respectively, which show that the as-synthesized InSe is more stable than BP, $MoTe_2$ and WTe_2.

can be directly distinguished in the experimental images due to their different atomic arrangements and contrast profiles. More importantly, we found that both β- or γ-InSe can co-exist in the CVD-grown few layer InSe which forms a stacking boundary, as shown in figure 4(d). The interface has an abrupt pattern change from β- to γ-InSe, suggesting an atomically sharp boundary between the two domains as highlighted by the red dashed line. The fast Fourier transform pattern (FFT) of the same region only shows one set of hexagonal spots, confirming the two sides share the same orientation. These abrupt stacking boundaries may modify the optical and electrical properties in the InSe matrix, as illustrated by similar structures in MX_2 structures [40, 41].

We also investigated the edges of InSe monolayer since the edge states have profound effect on the electronic structure. Figure 4(e) shows an atomic resolution STEM image of a free-standing fresh edge of InSe monolayer and the corresponding deconvoluted data for better visibility. The outmost two rows of atoms maintain lower intensity than the other atoms inside the film, which can be attributed to single Se and In atoms according to their contrast profile. Consequently, the edge forms distorted hexagons terminated by Se atoms, presumably due to the preferential lower energy configuration as capped by in-plane In–Se bonding instead of Se_2 or In_2 columns, as illustrated by the side view of the atomic model. Simulation using such structural model matches well with the experimental images, corroborating the occurrence of edge reconstruction. Such edge structure is dramatically different from the previously reported edges in bilayer GaSe which is terminated by Se_2 columns [42].

We explored the SHG effect in monolayer InSe under the non-resonant condition and compare it with monolayer WS_2, monolayer MoS_2 and monolayer GaSe (Supporting Information). Figure 5(a) shows the optical images of InSe that was used to explore the SHG. We selected the wavelength of ~800 nm as the excitation wavelength and investigated the dependence of SHG intensity on the laser excitation power, which are shown in figure 5(b). The strong SHG signal appears at 400 nm. The intensity of SHG increased with the laser excitation power increased from 1 mW to 8 mW. According to the electric dipole theory which predicts that under the first-order perturbation $I_{SHG} = |E(2\omega)|^2 \propto |P(\omega)|^2$, where I_{SHG}, $E(2\omega)$ and $P(\omega)$ are the SHG intensity, SHG electric field vector and excitation power, respectively, the SHG intensity should show a quadratic dependence on the excitation power. In our experiment, the measured intensity of SHG changes with different laser excitation power, and the square fitted result is shown in figure 5(c), consistent with theory calculation that the exponent is a value of 2. The optical second-order susceptibility was quantitatively estimated for monolayer InSe, the corresponding calculation formula same as the reported in other TMDs with the same structure is shown in supporting information. We found that the χ in monolayer is about 6.39×10^{-9}. To the best of our knowledge, it is the largest value reported so far, which is around 2 orders of magnitude larger than monolayer MoS_2, and even 3 times higher than the monolayer GaSe.

Based on the strong SHG signal, we further investigated the crystal structure of InSe by polarization-dependent SHG intensity. The intensity of SHG was detected with the emission field polarization parallel to the excitation field. Due to the three-fold symmetry in the monolayer InSe crystal structure, a six-fold rotational symmetry of SHG intensity were obtained with SHG intensity varying under different azimuthal angle theta (shown in figure 5(a)). The corresponding polarization-dependent SHG intensity is shown in figure 5(d), it can be seen that a clear six-petal pattern was obtained, which reveals the symmetry and orientation of the InSe monolayer. The intensity of the SHG

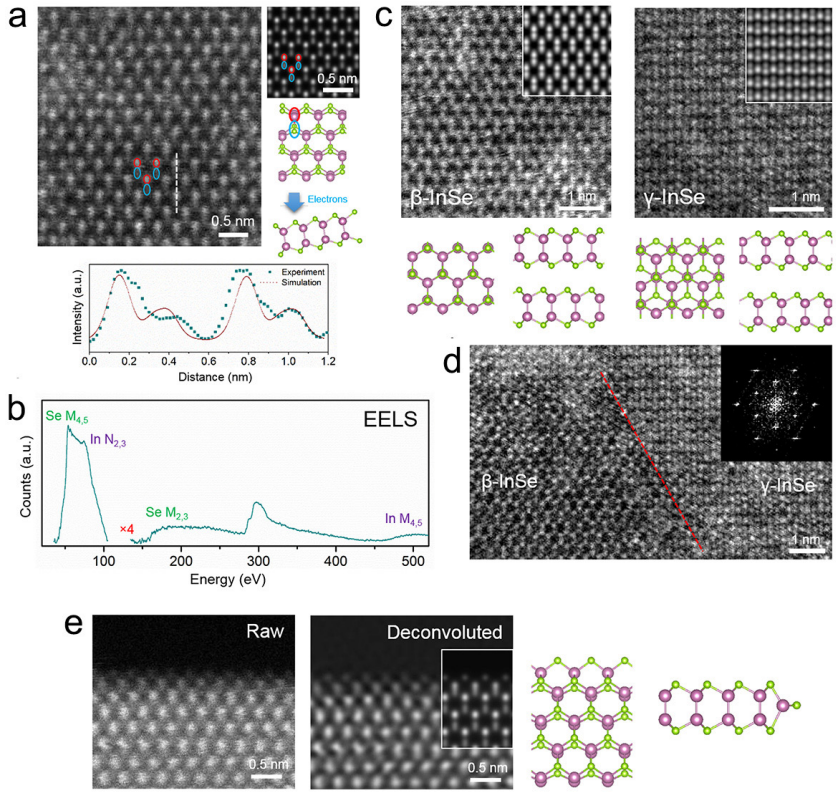

Figure 4. STEM characterization of InSe monolayer, stacking order and edges. (a) ADF-STEM image of monolayer InSe. The elliptical shape of the atomic columns comes from the displacement of the overlapping atoms due to the presence of a small tilting angle (~10°). Simulation and atomic structural models are provided on the right. The intensity profile along the highlighted white dashed line is also displayed below the image. (b) EELS spectrum of the monolayer InSe region. (c) ADF-STEM image of the β- and γ-InSe few layer with the simulated images overlaid. The structural models are provided underneath. (d) Atomically sharp stacking boundary between the β- and γ-InSe domains. FFT patterns show the same orientation on the two sides. (e) ADF-STEM and corresponding deconvoluted image of the reconstructed edge structure in a free-standing InSe monolayer. The simulation is overlaid. Atomic model is provided on the right. The edge is capped by in-plane In–Se bonding rather than Se_2 or In_2 columns.

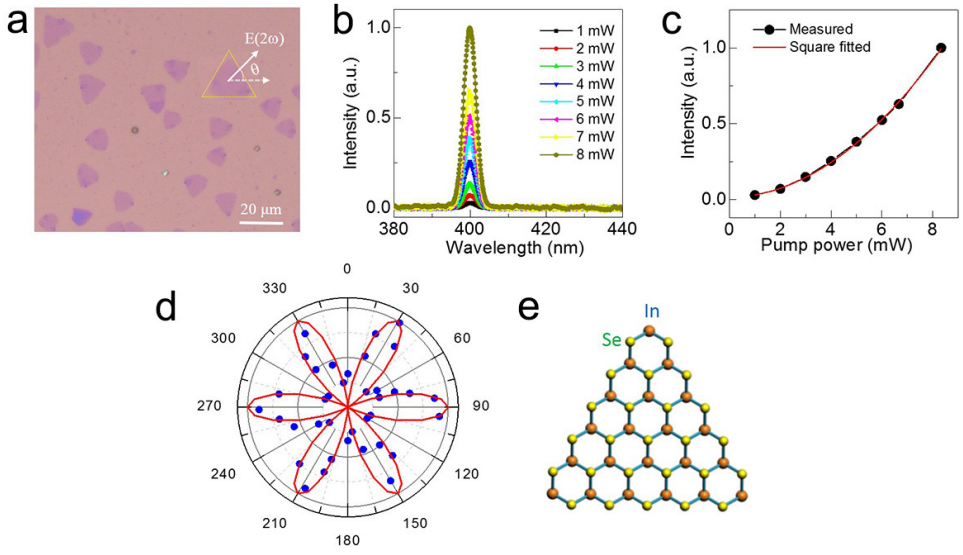

Figure 5. Second-harmonic generation in monolayer InSe. (a) Optical image of monolayer InSe. (b) SHG intensity dependency on the emission power. The SHG intensity increases as the power increased. The measured and square fitted of the intensity of SHG dependence of pump power are shown in (c). The exponent is about 2. (d) SHG intensity dependency on the azimuthal angle. The six-fold rotational symmetry suggests the three-fold symmetry in monolayer InSe as shown in (e), the atomic structure of the monolayer InSe.

dependence of the azimuthal angle can be describe by $I = I_0\mathrm{Sin}(\theta)$, where the I and I_0 are the SHG intensity and maximum intensity of SHG response, respectively. It can be seen that the maximum petal direction is parallel to the in-plain Se–In or In–Se direction, which cannot be distinguished due to the structure of

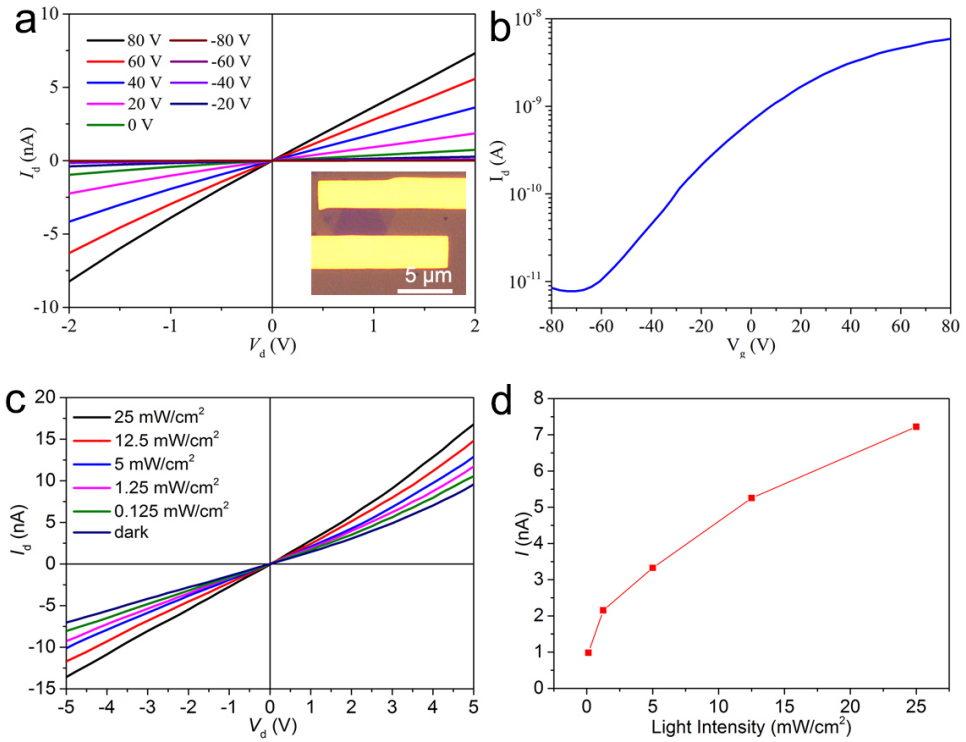

Figure 6. Optoelectronic performance of few-layer InSe. (a) Output characteristics of few-layer InSe (Inset: optical image of device). (b) Transfer curves of a few-layer InSe transistor. (c) and (d) Photocurrent as a function of the drain voltage under the illumination of different light intensities at a wavelength of 532 nm.

monolayer InSe. The corresponding possible structure model is shown in figure 5(e).

In order to further investigate the optical and electronic properties of InSe, FET devices were fabricated using the few-layer InSe. The Cr/Au (~5 nm and 50 nm, respectively) contacts as the drain and source were thermally evaporated onto the surface defined by electron beam lithography (EBL). The output and the transfer characteristics of the fabricated transistor are shown in figures 6(a) and (b), respectively. The results show that the InSe maintains an n-type semiconductor character and the FET device shows good contact under different drain and source voltages. The on/off ratio shown in figure 6(b) is about 10^3, better than the reported value in exfoliated InSe flakes [21].

We also investigated the photodetector properties in the few-layer InSe sample. Figure 6(c) shows the *I*–*V* characteristics of InSe photodetector measured under dark and different light intensity with 532 laser illuminated. The photocurrent reaches about 17 nA at light intensity 25 mW cm^{-2}. Notably, I_d shows strong photo response dependence on the incident light intensity (P), as shown in figure 6(d). From the equation photoresponsivity $= (I_{light} - I_{dark})/P_{light}$ and according to the result in figure 6(d), the photoresponsivity is calculated to be ~6 A W^{-1}, which is superior to other 2D materials such as graphene, GaS, and GaSe [16, 43, 44], further demonstrating InSe layers as an excellent candidate in optoelectronic applications.

Conclusions

In summary, InSe monolayers and few-layers were successfully synthesized via PVD method. The high quality was confirmed by various characterization techniques, and its atomic structure is investigated by high resolution ADF-STEM imaging. We found different stacking orders co-exist in the same film, connected by a sharp stacking boundary. Edge reconstruction with distinct atomic structure was also observed in monolayer InSe. The observed strong SHG signal arising from the InSe monolayer further revealed its SHG intensity dependence of the azimuthal angle, showing excellent optical second-order susceptibility. FET and photodetector fabricated using few-layer InSe shows high on/off current ratio and high photo-responsivity. All these results indicate the potential of InSe in the field of optoelectronic applications.

Acknowledgment

This work is supported by the Singapore National Research Foundation under NRF Award No. NRF-NRFF2013-08, the start-up funding from Nanyang Technological University (M4081137.070). JL and KS acknowledge JST-ACCEL and JSPS KAKENHI (JP16H06333 and P16823). XF Liu thanks the support from the 100-Talents Program of the Chinese Academy of Sciences (No. Y5862911ZX and No. Y5862912ZX).

Conflicts of interest

The authors declare no conflict of interest

ORCID iDs

Xinfeng Liu https://orcid.org/0000-0002-7662-7171
Zheng Liu https://orcid.org/0000-0002-8825-7198

References

[1] Radisavljevic B and Kis A 2013 Mobility engineering and a metal–insulator transition in monolayer MoS_2 *Nat. Mater.* **12** 815–20
[2] Li L K, Yu Y J, Ye G J, Ge Q Q, Ou X D, Wu H, Feng D L, Chen X H and Zhang Y B 2014 Black phosphorus field-effect transistors *Nat. Nanotechnol.* **9** 372–7
[3] Chen J H, Jang C, Xiao S D, Ishigami M and Fuhrer M S 2008 Intrinsic and extrinsic performance limits of graphene devices on SiO_2 *Nat. Nanotechnol.* **3** 206–9
[4] Novoselov K S, Jiang D, Schedin F, Booth T J, Khotkevich V V, Morozov S V and Geim A K 2005 Two-dimensional atomic crystals *Proc. Natl Acad. Sci. USA* **102** 10451–3
[5] Lopez-Sanchez O, Lembke D, Kayci M, Radenovic A and Kis A 2013 Ultrasensitive photodetectors based on monolayer MoS_2 *Nat. Nanotechnol.* **8** 497–501
[6] Perkins F K, Friedman A L, Cobas E, Campbell P M, Jernigan G G and Jonker B T 2013 Chemical vapor sensing with mono layer MoS_2 *Nano Lett.* **13** 668–73
[7] Yin Z Y, Li H, Li H, Jiang L, Shi Y M, Sun Y H, Lu G, Zhang Q, Chen X D and Zhang H 2012 Single-layer MoS_2 phototransistors *ACS Nano* **6** 74–80
[8] Xiao D, Liu G B, Feng W X, Xu X D and Yao W 2012 Coupled spin and valley physics in monolayers of MoS_2 and other group-VI dichalcogenides *Phys. Rev. Lett.* **108** 196802
[9] Novoselov K S, Geim A K, Morozov S V, Jiang D, Zhang Y, Dubonos S V, Grigorieva I V and Firsov A A 2004 Electric field effect in atomically thin carbon films *Science* **306** 666–9
[10] Najmaei S, Liu Z, Zhou W, Zou X L, Shi G, Lei S D, Yakobson B I, Idrobo J C, Ajayan P M and Lou J 2013 Vapour phase growth and grain boundary structure of molybdenum disulphide atomic layers *Nat. Mater.* **12** 754–9
[11] Cong C X, Shang J Z, Wu X, Cao B C, Peimyoo N, Qiu C, Sun L T and Yu T 2014 Synthesis and optical properties of large-area single-crystalline 2D semiconductor WS_2 monolayer from chemical vapor deposition *Adv. Opt. Mater.* **2** 131–6
[12] Wang X L *et al* 2014 Chemical vapor deposition growth of crystalline mono layer $MoSe_2$ *ACS Nano* **8** 5125–31
[13] Huang J K, Pu J, Hsu C L, Chiu M H, Juang Z Y, Chang Y H, Chang W H, Iwasa Y, Takenobu T and Li L J 2014 Large-area synthesis of highly crystalline WSe_2 mono layers and device applications *ACS Nano* **8** 923–30
[14] Lin Z *et al* 2016 2D materials advances: from large scale synthesis and controlled heterostructures to improved characterization techniques, defects and applications *2D Mater* **3** 042001
[15] Zhou Y B, Nie Y F, Liu Y J, Yan K, Hong J H, Jin C H, Zhou Y, Yin J B, Liu Z F and Peng H L 2014 Epitaxy and Photoresponse of two-dimensional GaSe Crystals on flexible transparent mica sheets *ACS Nano* **8** 1485–90
[16] Hu P A *et al* 2013 Highly responsive ultrathin GaS nanosheet photodetectors on rigid and flexible substrates *Nano Lett.* **13** 1649–54
[17] Tamalampudi S R, Lu Y Y, Kumar U R, Sankar R, Liao C D, Moorthy B K, Cheng C H, Chou F C and Chen Y T 2014 High performance and bendable few-layered InSe photodetectors with broad spectral response *Nano Lett.* **14** 2800–6
[18] Zhai T Y *et al* 2010 Fabrication of high-quality In_2Se_3 nanowire arrays toward high-performance visible-light photodetectors *ACS Nano* **4** 1596–602
[19] Feng W, Zheng W, Cao W W and Hu P A 2014 Back gated multilayer InSe transistors with enhanced carrier mobilities via the suppression of carrier scattering from a dielectric interface *Adv. Mater.* **26** 6587–93
[20] Bandurin D A *et al* 2017 High electron mobility, quantum Hall effect and anomalous optical response in atomically thin InSe *Nat. Nanotechnol.* **12** 223–7
[21] Lei S D *et al* 2014 Evolution of the electronic band structure and efficient photo-detection in atomic layers of InSe *ACS Nano* **8** 1263–72
[22] Lei S D *et al* 2015 An atomically layered InSe avalanche photodetector *Nano Lett.* **15** 3048–55
[23] Mudd G W *et al* 2015 High broad-band photoresponsivity of mechanically formed InSe-graphene van der Waals heterostructures *Adv. Mater.* **27** 3760–6
[24] Yin X B, Ye Z L, Chenet D A, Ye Y, O'Brien K, Hone J C and Zhang X 2014 Edge nonlinear optics on a MoS_2 atomic monolayer *Science* **344** 488–90
[25] Zhang Y J, Oka T, Suzuki R, Ye J T and Iwasa Y 2014 Electrically switchable chiral light-emitting transistor *Science* **344** 725–8
[26] Yu H Y, Wu Y, Liu G B, Xu X D and Yao W 2014 Nonlinear valley and spin currents from fermi pocket anisotropy in 2D crystals *Phys. Rev. Lett.* **113** 156603
[27] Zhou X, Cheng J X, Zhou Y B, Cao T, Hong H, Liao Z M, Wu S W, Peng H L, Liu K H and Yu D P 2015 Strong second-harmonic generation in atomic layered GaSe *J. Am. Chem. Soc.* **137** 7994–7
[28] Deckoff-Jones S, Zhang J J, Petoukhoff C E, Man M K L, Lei S D, Vajtai R, Ajayan P M, Talbayev D, Madeo J and Dani K M 2016 Observing the interplay between surface and bulk optical nonlinearities in thin van der Waals crystals *Sci. Rep.* **6** 22620
[29] Lin M *et al* 2013 Controlled growth of atomically thin In_2Se_3 flakes by van der Waals epitaxy *J. Am. Chem. Soc.* **135** 13274–7
[30] Zhou J D, Zeng Q S, Lv D H, Sun L F, Niu L, Fu W, Liu F C, Shen Z X, Jin C H and Liu Z 2015 Controlled synthesis of high-quality mono layered alpha-In_2Se_3 via physical vapor deposition *Nano Lett.* **15** 6400–5
[31] Lei S D, Ge L H, Liu Z, Najmaei S, Shi G, You G, Lou J, Vajtai R and Ajayan P M 2013 Synthesis and photoresponse of large GaSe atomic layers *Nano Lett.* **13** 2777–81
[32] Emery J Y, Brahimotsmane L, Jouanne M, Julien C and Balkanski M 1989 Growth-conditions of inxsey films by molecular-beam deposition *Mater. Sci. Eng.* B **3** 13–7
[33] Tedenac J C, Vassilev G P, Daouchi B, Rachidi J and Brun G 1997 Low-temperature region of the In–Se system *Cryst. Res. Technol.* **32** 605–16
[34] Balakrishnan N *et al* 2016 Quantum confinement and photoresponsivity of β-In_2Se_3 nanosheets grown by physical vapour transport *2D Mater.* **3** 025030
[35] Yang Z B, Jie W J, Mak C H, Lin S H, Lin H H, Yang X F, Yan F, Lau S P and Hao J H 2017 Wafer-scale synthesis of high-quality semiconducting two-dimensional layered InSe with broadband photoresponse *ACS Nano* **11** 4225–36
[36] Ryder C R, Wood J D, Wells S A, Yang Y, Jariwala D, Marks T J, Schatz G C and Hersam M C 2016 Covalent functionalization and passivation of exfoliated black phosphorus via aryl diazonium chemistry *Nat. Chem.* **8** 598–603
[37] Zhou J D *et al* 2017 Large-area and high-quality 2D Transition metal telluride *Adv. Mater.* **29** 1603471
[38] Krivanek O L *et al* 2010 Atom-by-atom structural and chemical analysis by annular dark-field electron microscopy *Nature* **464** 571–4

[39] Debbichi L, Eriksson O and Lebegue S 2015 Two-dimensional indium selenides compounds: an *ab initio* study *J. Phys. Chem. Lett.* **6** 3098–103
[40] Lin J H, Pantelides S T and Zhou W 2015 Vacancy-induced formation and growth of inversion domains in transition-metal dichalcogenide monolayer *ACS Nano* **9** 5189–97
[41] Zhou W, Zou X L, Najmaei S, Liu Z, Shi Y M, Kong J, Lou J, Ajayan P M, Yakobson B I and Idrobo J C 2013 Intrinsic structural defects in monolayer molybdenum disulfide *Nano Lett.* **13** 2615–22
[42] Li X F *et al* 2015 Revealing the preferred interlayer orientations and stackings of two-dimensional bilayer gallium selenide crystals *Angew. Chem., Int. Ed.* **54** 2712–7
[43] Sun D, Aivazian G, Jones A M, Ross J S, Yao W, Cobden D and Xu X D 2012 Ultrafast hot-carrier-dominated photocurrent in graphene *Nat. Nanotechnol.* **7** 114–8
[44] Hu P A, Wen Z Z, Wang L F, Tan P H and Xiao K 2012 Synthesis of few-layer GaSe nanosheets for high performance photodetectors *ACS Nano* **6** 5988–94